Spring 2023

Stratigraphic Architecture of Pozuelo Mounds as Revealed by Earth Resistivity Tomography

Caeli Connolly

STRATIGRAPHIC ARCHITECTURE OF POZUELO MOUNDS AS REVEALED BY EARTH RESISTIVITY TOMOGRAPHY

by

Caeli Connolly

A Thesis Submitted in Partial Fulfillment
Of the Requirements for a Degree with Honors
(Earth and Climate Science)

The Honors College

University of Maine

April 2023

Advisory Committee:

Dr. Daniel Sandweiss, Professor of Anthropology and Quaternary and Climate Studies, Cooperating Professor of Earth and Climate Sciences and Global Policy, Advisor

Dr. Katherine Allen, Associate Professor School of Earth and Climate Sciences, Cooperating Appointment, Climate Change Institute and School of Marine Sciences

Dr. Allen Gontz, Professor of Applied Geology, Clarkson University

Dr. Alice Kelley, Emerita, Instructor School of Earth & Climate Sciences and Associate Research Associate Professor Climate Change Institute, Cooperating Assistant Professor of Anthropology

Dr. Jiaze Wang, Assistant Professor, School of Earth and Climate Sciences

ABSTRACT

This study is a geoarchaeological analysis using earth resistance tomography (ERT) surveys of two of four mounds at Pozuelo (Formative Period, cal yr 3000 BP) in the Chincha Valley of coastal, southern Peru. Layers identified in the subsurface were to determine the presence or absence of regional continuity between the mounds. This effort is part of a larger investigation examining the paleoenvironmental setting of the site, and its influence on site location and use. Ten earth resistance tomography profiles were collected using an ABEM Terrameter LS2 and 81 pin array. These profiles were then topographically corrected using topographic survey data collected with a Sokkai auto level and a metric Philadelphia rod as part of this study. This thesis looks to relate the ERT subsurface structures between two of the site's four mounds (B and D) and connect the ERT structures to the stratigraphic layers observed in a 4 meter deep excavation pit in Mound D. Specific layers observed in the Mound D stratigraphy, aeolian sand and blocky clay, were identified on the ERT data, but a consistent correlation between the ERT data and stratigraphy could not be established. An older mound was identified within Mound B, and its boundary was drawn using the collected ERT data. Due to the inability to establish a direct correlation between the Mound D stratigraphic column and the ERT data, subsurface layers between Mounds B and D were not identified.

TABLE OF CONTENTS

LIST OF FIGURES

INTRODUCTION

Site Location

The Pozuelo archaeological site is located in the Chincha Valley, along the coast of Southern Peru (13 34.312'S, 76 10.260'W). A series of four mounds make up the site, shown in figure 1: from north to south, Mound A, Mound B, Mound C, and Mound D (Figure 1). Research for this study investigates Mounds B and D. Chicken coops have been built on top of Mound C, making it inaccessible to ERT surveys and excavation. Irrigated farmland surrounds the mounds. The low-lying area surrounding the mounds is used to grow beans, corn, and asparagus. Mound material has been destroyed by agricultural practices, particularly around the mound edges and on the mound tops. Figure 1 shows bulldozer tracks along the top of Mound D, where the cultural mound material has been removed from the top of the mound and spread out over the fields. Excavation pit unit 31 was dug on Mound D by Christine Bergmann of the University of South Florida and its location is shown in figure 2.

Figure 1. Map of Pozuelo Site: The four mounds that make up the Pozuelo site are labeled. The red box that defines the site shows the location of the site in the Chincha Valley, Peru. Images are from Google Earth.

Geology of Area

Information on the geology of the Chincha Valley was taken from the 1970 map of the San Juan and Topará river basins. The Chincha Valley, including Pozuelo, is largely filled in by an alluvial fan. Sediments at the Pozuelo site are mainly sand, gravel, and clay. These sediments are likely the material that were used to construct the mound. Fine grained sediments of marine origin are also seen in the alluvial plain. These calcareous sediments are a possible source of the calcite nodules found in the clay layer of unit 31. Another possible source of calcite is the massive limestones located in the foothills of the Andes to the east of the site. This calcite from the massive limestones could be transported through the river and groundwater to the Pozuelo site. The basement

bedrock of the area is Andean granite, which includes granite, granodiorites, diorites, and tonalites. There is also andesitic rock of volcanic origin in the foothills of the Andes.

Cultural History of the Area

The Paracas culture is a pre-Hispanic Andean society located along the southern coast of Peru from 800 BCE to 200 BCE (Tantaleán 2021; Tantaleán et al. 2016). Paracas sites have been found along the coast and up into the foothills of the Andes. Spread across the various valleys (Cañete, Topará, Chincha, Pisco, Ica, and the valleys in the Rio Grande Basin), each Paracas community had their own architectural and artisanal features and functioned with their own political and economic systems (Tantaleán 2021). While the Chavin culture, which functioned more like a religious cult, is older, Paracas is the first regional culture to develop on the southern coast of Peru (Silverman 1996). The Paracas people were connected through a shared religious ideology and long distance trade. Religious practice for the Paracas people centered around the Oculate Being (Silverman 1996). Long distance trade includes items include obsidian and marine resources (Silverman 1996).

Paracas culture is divided into three different geographic sections (north, central, south) and three different time periods (Phase I 840-500 BCE, Phase II 500-380 BCE, Phase III 380-260 BCE) (Tantaleán 2021). Chronology of the Paracas culture is largely established on the basis of distinctive changes in pottery style. The Ocucaje sequence features 10 pottery phases that are used to establish a timeprofile of Paracas cultural evolution (Tantaleán et al. 2016; DeLeonardis 2005; Strong 1957). Field work has allowed archaeologists to best define and understand Ocucaje phases 3, 4, 6, 7, 8, 9, and 10 (DeLeonardis 2005). Early Paracas culture is less understood compared to the later

phases due to a lack of older sites. One cause of this may be the Paracas tradition of constructing new mounds on top of the preexisting structures. Fernando Herrera found evidence of older Paracas pottery in the fill and adobe bricks of a mound structure at the Alto del Molino site, in the lower Pisco Valley (Silverman 1996). Other archaeologists have suggested that the earlier Paracas cultures may lack above ground structures or have been concealed or destroyed by later occupation (DeLeonardis 2005). The Paracas culture began to collapse after 200 BCE, likely due to a drought and increased social conflict (Tantaleán 2021).

Paracas sites in the Chincha Valley span from larger monumental mounds to smaller platform mounds (Tantaleán et al. 2016), and spans the entire 800 BC to 200 BCE Paracas culture period. Evidence suggests Pozuelo was occupied during Phase I of the Paracas culture (Tantaleán 2021). Excavations began at Pozuelo in 2011 by Charles Stanish and Henry Tantaleán. Work at this site continued to the present. Evidence of weaving and pottery artifacts have been found at Pozuelo (Atwood 2020).

Earth Resistance Tomography and its Applications in Archaeology

Earth resistance tomography (ERT) is a noninvasive, geophysical data collection technique. It is used to image vertical stratigraphy and horizontal differentiation of the subsurface (Papadopoulos et al. 2014). Equipment required for ERT include an ammeter, voltmeter, power source, electrodes, connectors, and wire (Burger et al. 2006). The electrodes are metal stakes pounded into the ground and then attached to the wire with a connector (Burger et al. 2006). The wire is connected to the ammeter and voltmeter unit, which is connected to the power source. An electric current is then sent through the wire down a series of pins and passed to each pin through dissolved ions in the groundwater:

from pin 1 to pin 2, pin 1 to pin 3, etcetera until pin 1 sends electricity to the last pin in the profile (Di Maio et al. 2016; Linford 2006). Then pin 2 sends the current to pin 3, then pin 2 to pin 4, and so on until electricity is passed between all the pins in the transect profile. The result is that the system measures the potential difference between two points on the surface (Lascano et al. 2003). This creates a trapezoid of data as energy is sent into the ground and returned to the ammeter and voltmeter (figure 2).

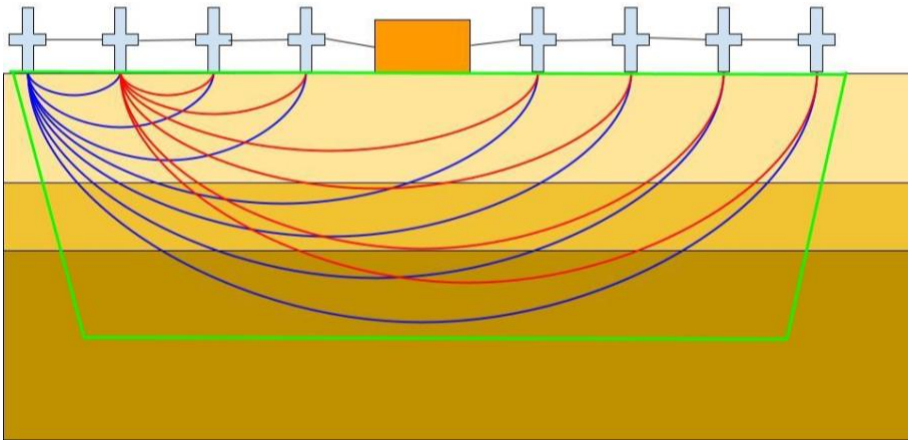

Figure 2. Schematic of ERT Data Collection: This diagram demonstrates how the electric current is passed from pin to pin through the subsurface.

The depth of information recorded is based on the spacing of the electrodes. For high resolution data over a shallow depth, the electrodes are spaced close together, for example 0.5 m spacing. Since the electric current does not have to travel far to get to each pin, a shallower depth profile is created. This creates a higher resolution data set. Using a larger electrode spacing, such as 5 m spacing, greater depths can be recorded since the path the electricity travels to reach each pin has a greater trajectory. The greater depth allows for more of the subsurface to be surveyed. This is demonstrated in figure 3.

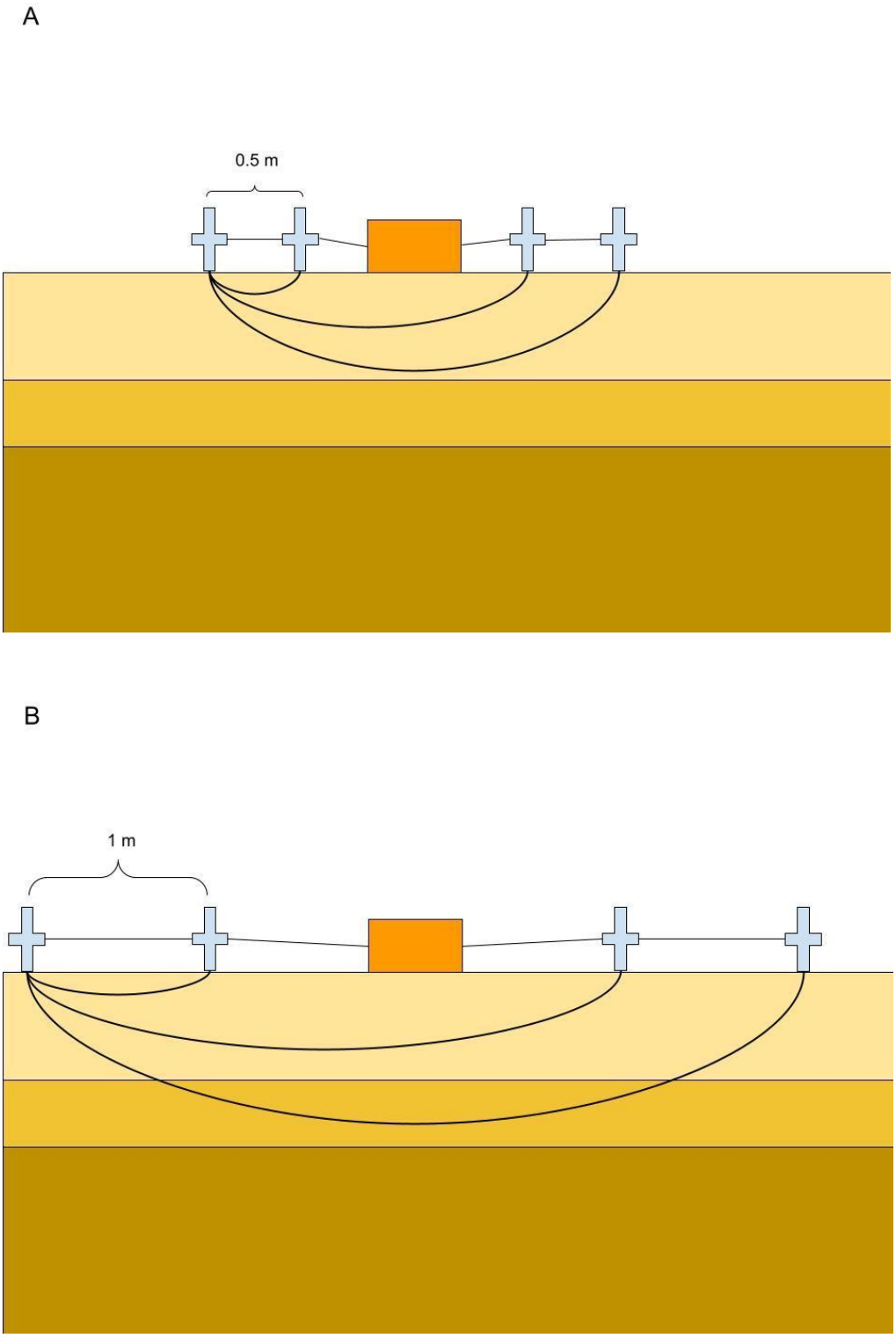

Figure 3. Schematic of ERT Depth of Data Survey: A) The pins are spaced at 0.5 m, allowing for shallow data collection. B) The pins are spaced at 1 m, giving the survey a greater depth of data collection.

Since geologic materials have different resistivity to electricity, the ERT is able to record variations in resistivity to determine subsurface structure (Burger et al 2006). A material's resistivity depends on the properties of that material, such as porosity, and shape (Linford 2006; Papadopoulos et al. 2014). Materials such as clay and silt have a lower resistivity compared to sands and gravels due to their smaller grain size (Burger et al. 2006). Increased water content and salinity of the water will also decrease a material's resistivity (Burger et al. 2006; Linford 2006; Young and Droege 1986). The presence of metallic minerals in the material also causes a lower resistance to the flow of the electric current. Generally shales, clays, salt and contaminated water, and sulfide and metallic ores are geologic materials with a low resistivity value (Burger et al. 2006). Geologic materials with high resistivity include limestone, dolomite, evaporites, and quartz-rich rock (Burger et al. 2006).

Earth resistance tomography has been used successfully in previous research to study archaeological sites in various settings. Due to fast data collection, ERT makes archaeological prospection more efficient by narrowing down the area of interest (Drahor et al. 2007; Drahor et al. 2008). Using ERT in the field to image the subsurface can offer information that other geophysical tools and invasive archaeological methods cannot supply (Kvamme 2006; Viberg et al. 2011). ERT can locate buried archaeological features in three dimensions such as walls, foundations, ditches, middens, and hearths (Lascano et al. 2003; L. Nuzzo et al. 2009; Drahor et al. 2007). It also allows geologic features like paleochannels to be mapped (Papadopoulos et al. 2014; Zheng et al. 2013). One limitation of ERT is that soil variations can sometimes hide archaeological features

(Young and Droege 1986). Three different archaeological case studies that use ERT to map the subsurface are examined in closer detail in the following paragraphs.

A study of the Jinsha site in Chengdu third ring, Sichuan Province, China, conducted by Zheng et al. in 2013 found ERT data could be correlated to the stratigraphic data from excavation units. The researchers used a high density resistivity method with a sixty electrode array and sixteen different electrode spacings to get various depth resolutions. Induced polarization method, multi frequency electromagnetic method, and ground penetrating radar were also used to survey at Jinsha. Based on the different electrical resistivities of rock and soil, the researchers were able to use the ERT data to identify the stratigraphic layers of the subsurface across the site. Using the distribution, thickness, and shape of the various sand, gravel, and silt layers, the researchers were able to locate paleo-river channels that ran through the Jinsha site (Zheng et al. 2013). The induced polarization and multi-frequency electromagnetic methods were able to locate bronze artifacts through weak anomaly signals. Ground penetrating radar surveys helped to survey the extent of cultural material. The combination of the various geophysical techniques allowed the researchers at Jinsha to perform medium- and large- scale surveys both to gain information about the entire site and to focus studies on specific locations to find artifacts.

In Floridablanca, an archaeological site in southern Argentina, Osella et al. in 2005 used electrical and electromagnetic methods to perform geophysical studies. The combination of the electrical and electromagnetic surveys was used to create a map of the buried, subsurface settlement structures of the 18th century site. The researchers used the resistivity and GPR surveys correlated with data from past excavations to determine the

location of adobe walls and collapsed roofs. This information was then applied to the resistivity surveys done in the southwest sector. The researchers used electrical and electromagnetic resistivity survey methods as thich vegetation ground cover was thick, preventing the use of GPR since ground contact could not be maintained across the entire transect. Two houses were mapped using the resistivity methods (Osella et al. 2005). Main structure walls, interior walls, and walls separating adjacent houses were identified in the data. The presence of collapsed roofs was determined due to the distinctive signal of the tiles on both the electrical and electromagnetic data. Using the geophysical survey methods allowed for Floridablanca to be mapped without excavation in the southwest sector, preserving the archaeological value of the site. The geophysical surveys also produced information on the paleoenvironment through the identification of geologic deposits and buried landforms.

Di Maio et al. in 2016 conducted research at Phaistos, an archaeological site in Crete, Greece, and used electrical resistance tomography, electromagnetic resistivity, and magnetic surveys to map the subsurface of the site. Phaistos is an important site in Greek archaeology, as it was used from Minoan through Roman periods. Uncultivated fields and olive trees in some parts of the site make aerial sensing and archaeological reconnaissance unsuitable methods for surveying. The clay rich soil also made GPR difficult to use, since the radar signal does not easily pass through clay. EM, ERT, and magnetic surveys provided the researchers with a fast and efficient way to survey large portions of the less excavated hills at Phaistos. Researchers found the geophysical surveys were able to provide information on the depth of the soil-bedrock interference, thickness of stratigraphic layers, and location and of archaeological features (Di Maio et

al. 2016). When compared, the different geophysical surveys showed similar structures, allowing a limestone wall to be identified and excavated with accuracy.

METHODS

At Pozuelo, the team used shallow earth geophysical systems, topographic profiling, GPS surveying and direct observation through excavation to characterize the site and develop an understanding of the subsurface architecture and correlation of features across the site. All data were integrated in geospatial software packages for visualization and interpretation.

Earth Resistivity Tomography

An ABEM Terrameter (LS2) with an 81 pin array was used to image the subsurface architecture. The LS2 did not collect inversed polarity (IP) data as the remote site did not have obvious sources of electrical interference. The system used a 0.5s measuring window for each iteration. Based on the site and areas of interest, a dipole-dipole sampling routine was used for all ERT profiles. Four cables with 5 m takeouts were available. For pin spacings less than 5 m, excess cable was coiled off the profile axis to accommodate the shorter interval. The setup utilized between 2 and 6 cables, with 2, 3 and 4 cable sets operating as one survey and the 5 and 6 cable sets were accomplished using the roll along feature of the LS2. The pins were spaced 0.5 to 2 m apart, depending on depth penetration and resolution desired. Due to a system malfunction in the field, the data for profiles 10 and 14 were corrupted and the data lost.

GPS Surveying

GPS data were collected for each profile using a handheld Garmin E-Trex10 unit. The number of GPS points recorded for each profile varied depending on the orientation of the survey profile. Points were recorded at endpoints, cable connections, locations where profiles crossed and where changes in profile orientation occurred. The GPS data

were plotted in Google Earth and used to spatially reference ERT profiles in Aarhus Workbench.

Topographic Profiling

Topography data were collected using a Sokkai auto level with a metric Philadelphia rod. Measurements were recorded for every pin in the ERT survey profiles, corners of excavations, and other key features. All elevations were referenced to a local benchmark set to an elevation of 100 m to develop relative topography and relate features across the site and recorded to 0.01 m. The topography data were then applied to the ERT profiles in a post processing software system.

Post Processing and Data Integration

ERT data were post-processed using Aarhus Workbench (AW). Data were downloaded from the LS2 via USB drive and transferred to the processing computer. Each profile was imported, topographic and spatial data were converted to AW-compatible format, and were then linked to the ERT profiles. All profiles were imported into the same workspace to facilitate analysis. Post inversion, data outputs were scaled to highlight the vertical differences and take advantage of the close pin spacing and high-resolution. Apparent resistivity values were displaced using a continuous color ramp based on natural breaks. The bin with the highest resistivities contained all readings with values greater than 200 mS. This served to filter out anomalous readings while preserving readings associated with geological and archaeological materials.

RESULTS

In June of 2022, our research team spent 10 days in the field collecting ERT data at Mound B and Mound D and conducting stratigraphic analysis at an open excavation pit, unit 31, at Mound D. In this study, the ERT profiles located over Mounds B and D and the surrounding, low-lying fields (Figure 4) were evaluated. Data analysis for the ERT profiles collected on Mound D focused on establishing a correlation between the stratigraphic layers seen in unit 31 and the subsurface layers seen in the ERT profiles. On Mound B, analysis focused on determining the presence and boundary of a mound-within-mound structure. Both horizontal and vertical distances are used to describe the ERT profiles. The H is used to denote horizontal distance and the V is used to denote vertical depth.

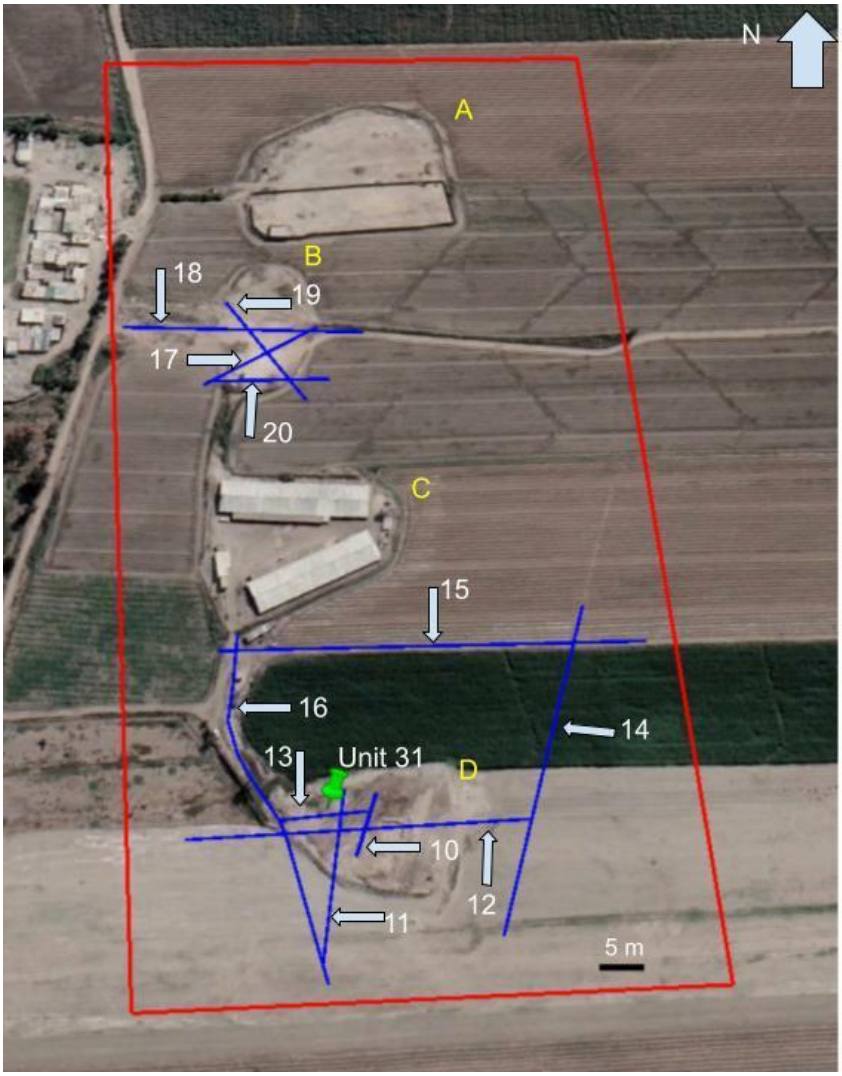

Figure 4. Map of ERT survey profiles: This map shows the labeled ERT profiles collected over Mound B, Mound D, and the surrounding low-lying fields. The location of unit 31 is marked by the green pin. Image is from Google Earth.

Mound D ERT Profiles

Five of the ten ERT profiles were collected over mound D (Figure 4). The data for profile 10 were corrupted due to a system malfunction in the field and were not able to be processed or analyzed. Profiles 11, 12, 13, and 16 were used to establish a correlation between the subsurface layers observed in the ERT data and the stratigraphy of Mound D. Profile 13 and 16 were reprocessed to show only the top 5 m of the data profile and are shown in figure 5 in order to create higher resolution ERT profiles.

Profile 11 was oriented from north to south over top of the mound (Figure 5A). The majority of the ERT profile shows the surfaces having a higher resistivity value, purple color, with the exception of a lower resistivity section from 20-30 m H. In the area of lower resistivity there is a section of higher resistivity, the red color on the surface, at 24.5 m H. The purple arrows at 27.5 m H and 29.5 m H point to two areas of lower resistivity, indicated by the green color, that appear to have identical signals.

Profile 12 was positoned from east to west over Mound D (Figure 5B). The profile 12 data do not show the topography recorded in the field. The brown arrows mark the locations of the mound boundary edges. The surface of profile 12 has high resistivity values shown in the purple layer. The higher resistivity extends deeper into the subsurface from 52-72 m H. Deeper within the subsurface there are pockets of lower resistivity indicated by the green layers and areas of light and dark blue.

Profile 13 was oriented from east to west over Mound B (Figure 5C). The first 20 m H of profile 13 show a continuous lower resistivity layer on the surface, green, with a discontinuous higher resistivity layer below, red and purple signal, at 8m H and again from 10-16 m H. After 20 m H, the surface has a much higher resistivity indicated by the appearance of the purple layer. Below this purple layer is a continuous layer with low resistivity seen in the light and dark blue signal color. With the exception of 13-18 m H, the bottom layer of the data profile has a higher resistivity value indicated by the purple and red.

The site featured a topographic high to the west of the cornfield to Mound D. Profile 16 followed the topographic high from the road, across the western edge of the mound, and down onto the surrounding low-lying field (Figure 5D). Generally, profile 16

was oriented from north to south. The blue arrow at 78 m H highlights a high resistivity signal in the irrigation channel that cuts through the topographic high. Mound D runs from 82-110 m H in the resistivity profile. From 82-92 m H, the mound has a high surface resistivity, purple, followed by a blue, low resistivity layer. Beneath that layer is a red high resistivity layer. The resistivity signal becomes low again, with the deep green layer. At 92 m H there is a shift in the resistivity signals of Mound D. There is a small area of low resistivity on the surface from 92-98 m H that is green in color. The remaining surface of the mound, 98-110 m H, is purple showing a higher resistivity value. Beneath the surface layers there is a deep high resistivity layer that has a red color, with a very high purple resistivity signal at 104 m H.

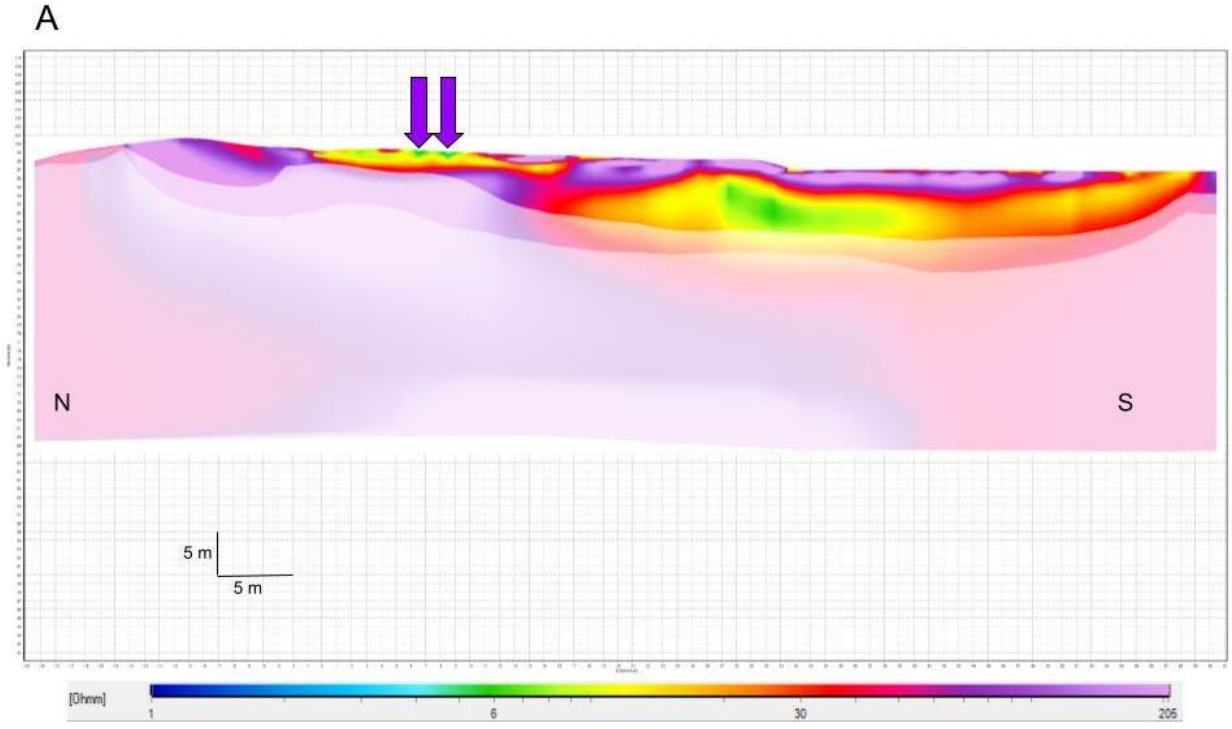

B

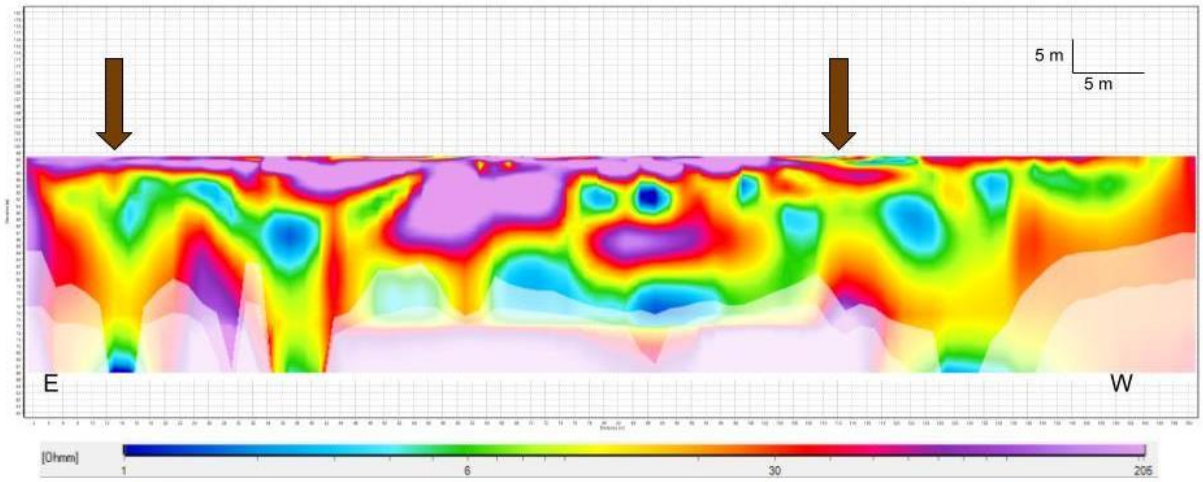

C

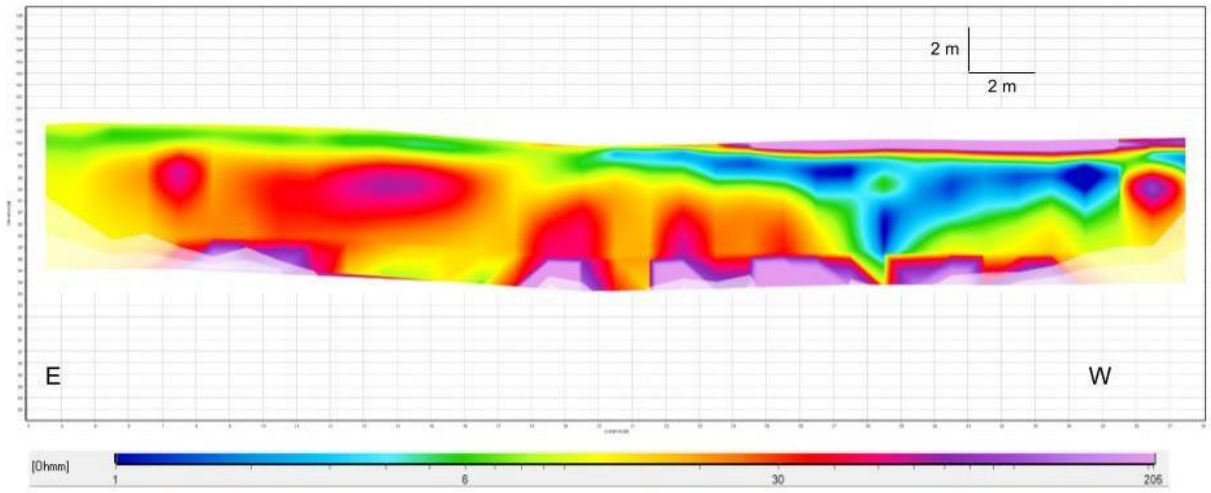

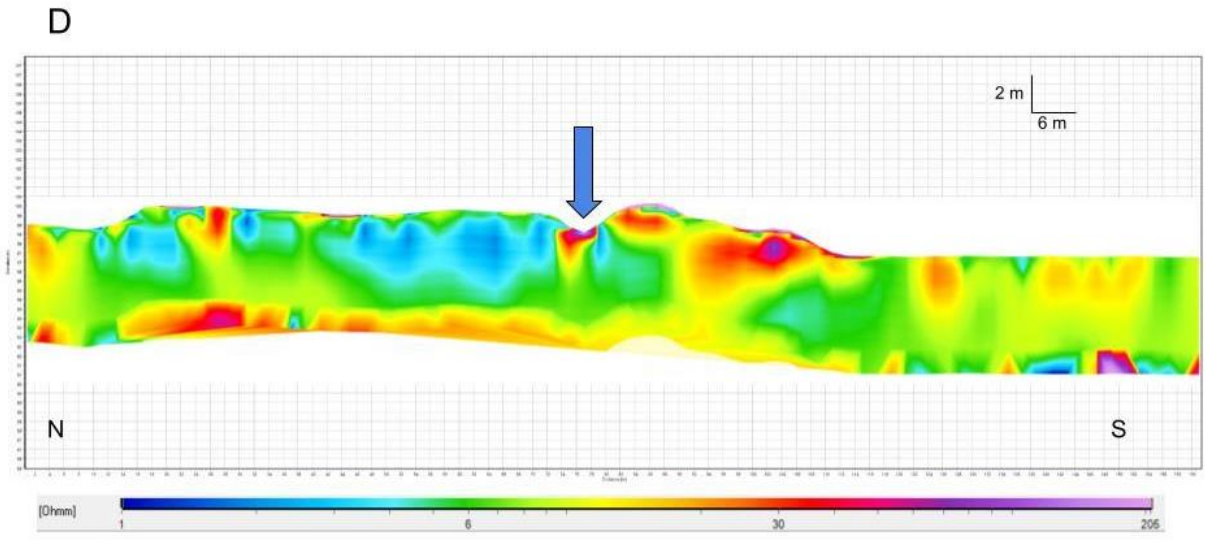

Figure 5. Mound D ERT Data: A) Profile 11, purple arrows pointing to possible wall signatures. B) Profile 12, brown arrows marking Mound D edges. C) Profile 13, reprocessed to 5 m deep. D) Profile 16, reprocessed to 5 m depth.

Mound B ERT Profiles

Preliminary investigation of the Mound B data in the field suggested that there may be a mound-within-mound structure present. Four ERT survey profiles were run over Mound B: profiles 17, 18, 19, and 20. Each profile was preprocessed to show only the top 5 m of the data and are shown in figure 6, to create higher resolution over mound structure.

Profile 17 was run diagonally over Mound B, from the southeast corner to the northwest corner of the mound (Figure 6A) . At 26 m H, profile 17 shows a distinct change in resistivity of the subsurface material, marked by the orange arrow. To the left of the 26 m H arrow, the material has a high resistivity indicated by the red and purple colors. On the right side of the 26 m H arrow, the resistivity values are lower, shown by the yellow, green, and blue colors. The purple arrows at 6 m H and 8 m H highlight two

areas of lower resistivity. On the northeast end of the profile, the ERT survey continued down off the mound and revealed a higher resistivity signal at 58 m H.

The data of profile 20 shows a similar pattern to profile 17. Profile 20 was positioned from west to east across the southernmost portion of Mound B (Figure 6B) . At 36 m H, there is a switch in resistivity of the mound material, marked by the orange arrow. The portion of the mound to the left of the 36 m H has higher resistivity values, shown by the red and purple colors. The right side of the orange arrow has portions of lower resistivity seen in the yellow, green, and blue colors. At 19 m H and 21 m H, there are small yellow signals.

Profile 18 was oriented from west to east along the access road that crossed over the top of Mound B (Figure 6C). At 77 m H, there is a slight change in resistivity values. To the left of the orange arrow at 77 m H there are higher resistivity values seen in the subsurface in the band of purple and red colors. A green and blue lower resistivity signal appears on the surface to the right of the orange arrow. The red and purple band does not continue in the subsurface to the right of the 77 m H distance. The blue arrow at 100 m H points to an area of high resistivity along the edge of the mound.

Profile 19 was positioned diagonally across the mound from the southeast corner to the northwest corner (Figure 6D). There is one area of distinct resistivity change at 24 m H marked by the leftmost arrow. The second orange arrow displays only a slight change in resistivity at 43 m H. A higher resistivity signal is seen at 8 m H. There is a blue area of lower resistivity from 8-13 m H on the southwest side of profile 19. The yellow arrow at 58 m H indicates the signal change showing lower resistivity in the subsurface.

A

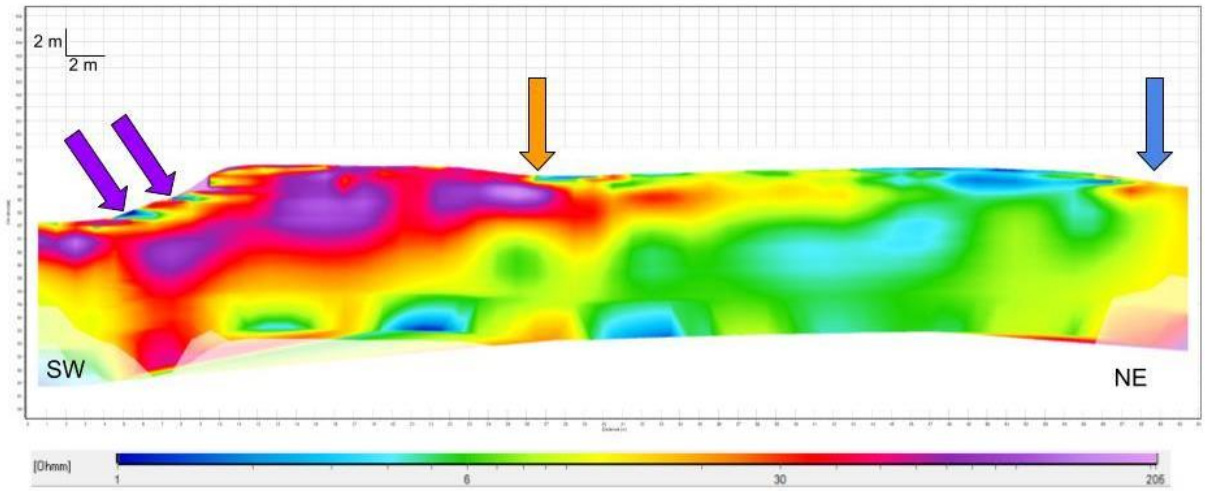

B

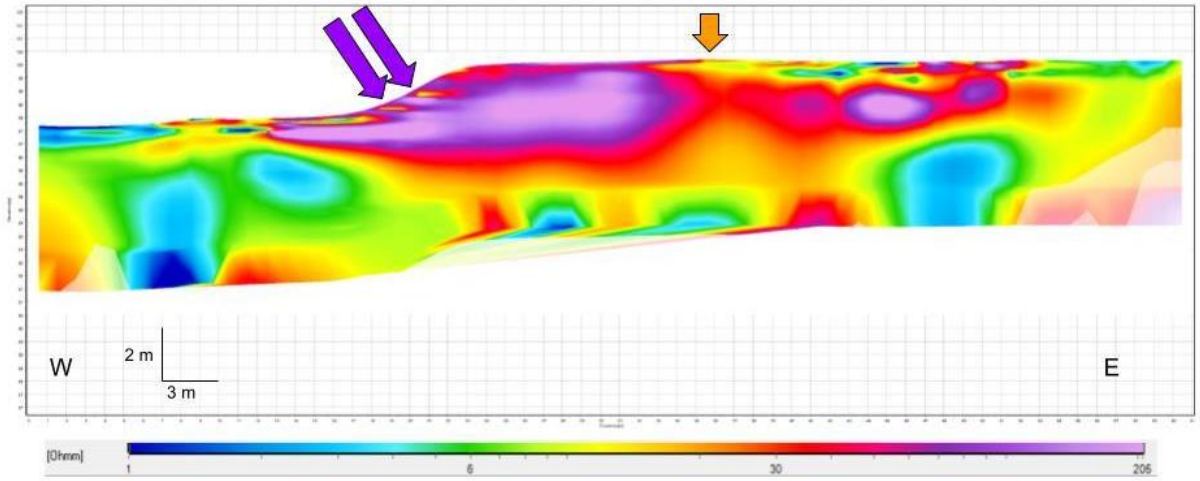

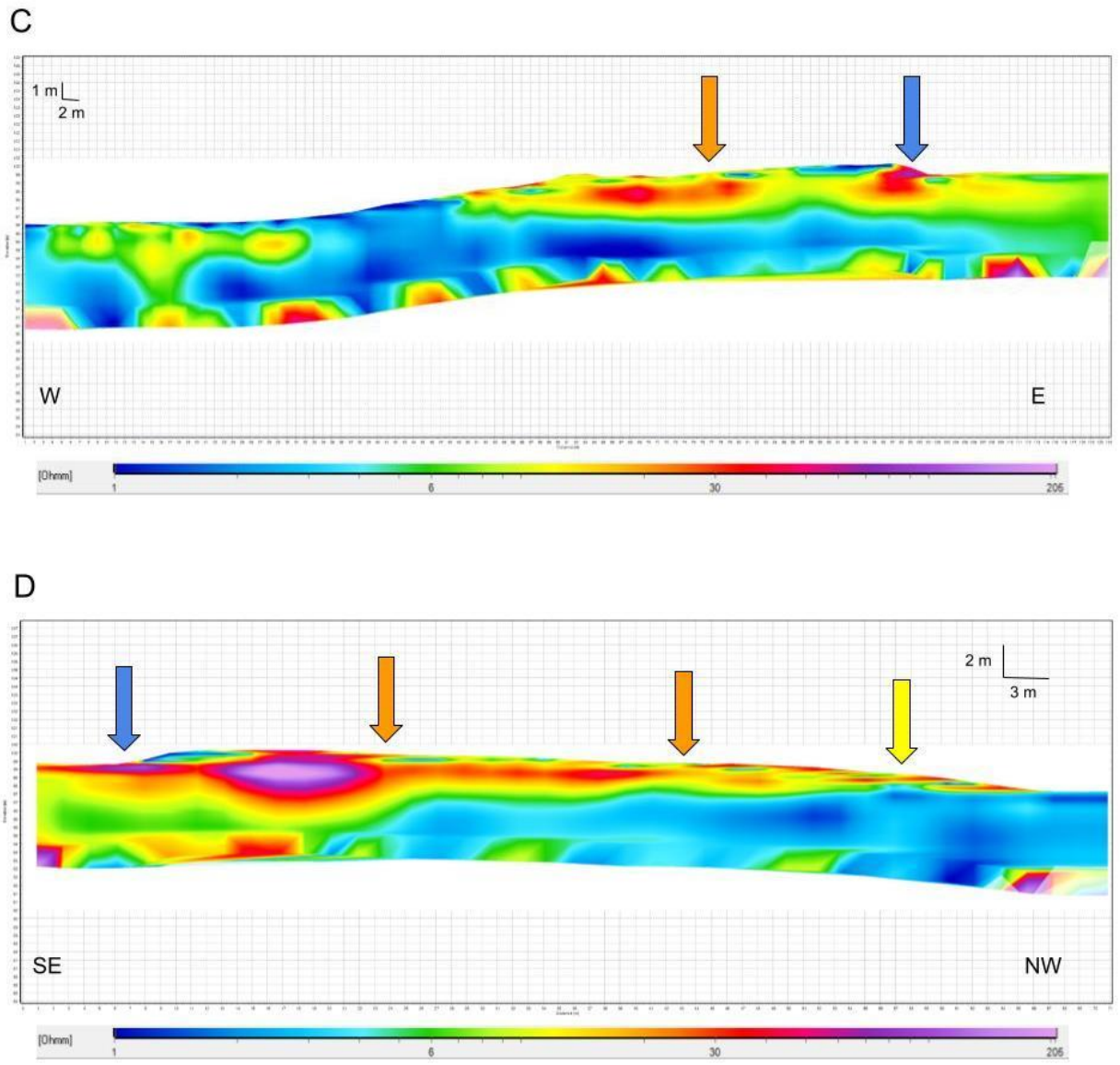

Figure 6. Mound B ERT Data. All profiles were reprocessed to a depth of 5 m. The purple arrows point to the signature of the adobe wall. The orange arrows indicate the mound-within-mound boundary location. The blue arrows show spots of high resistivity from irrigation water. The yellow arrow shows the signature of the brick wall. A) Profile 17 B) Profile 20 C) Profile 18 D) Profile 19

DISCUSSION

Mound D: Correlation Between Subsurface ERT and Mound Stratigraphy

The changes in resistivity of the different layers of Mound D indicate the various stratigraphic layers that make up the mound. Higher resistivity layers, indicated in the data by the red and purple colors, have a sandy composition. The lower resistivity sections of the mound, layers with green and blue colors, suggest materials that are rich in clay.

Unit 31 was excavated in the May 2022 field season by colleagues from University of Southern Florida. Original stratigraphic layers were drawn and labeled by Christine Bergmann in May. Updated stratigraphic columns were drawn in June by Dr. Alice Kelley and Elizabeth Leclerc. The basal unit is a blocky clay approximately 1 m V thick. This bottom layer of the excavation pit is intruded by clastic (sand) dikes and sand boil materials that create a 0.2 m V thick layer on top of the blocky clay. Another, thinner, clay layer settles out on top of the sand boil layer. A large, fine grained sand layer, possibly aeolian in origin, rests on top of the thin clay layer and is about 0.40-0.65 m V deep, thinning to the north. On top of the sand is another thinner clay layer that may be natural or cultural, approximately 2 m V deep. The remaining material ranges from sand and silt to silty clay and clay and are the result of human deposition to construct the mound. These layers feature inclusions of cultural material, such as pottery sherds and cultural floors.

From 3-20 m H, profile 13 ERT data (figure 5C) suggests a clay sediment layer approximately 1 m V deep and below this layer a sand-rich layer approximately 2 m deep. Using Google Earth plotted locations of unit 31 corners in relation to profile 13, the

pit should correlate to the area between 13-18 m H on profile 13. The area of profile 13 that aligns with the pit does fit with the Mound D stratigraphy (figure 7). The Mound D stratigraphy should show a layer of low resistivity on the surface, then a layer of higher resistivity, and on the bottom another low resistivity layer. The depths of the resistivity layers do not perfectly correlate to the thickness of the unit 31 stratigraphy, due to ERT being a non-unique solution. The ERT has a lower resolution so the boundaries between different stratigraphic layers are fuzzy and thin sediment layers may not appear at all.

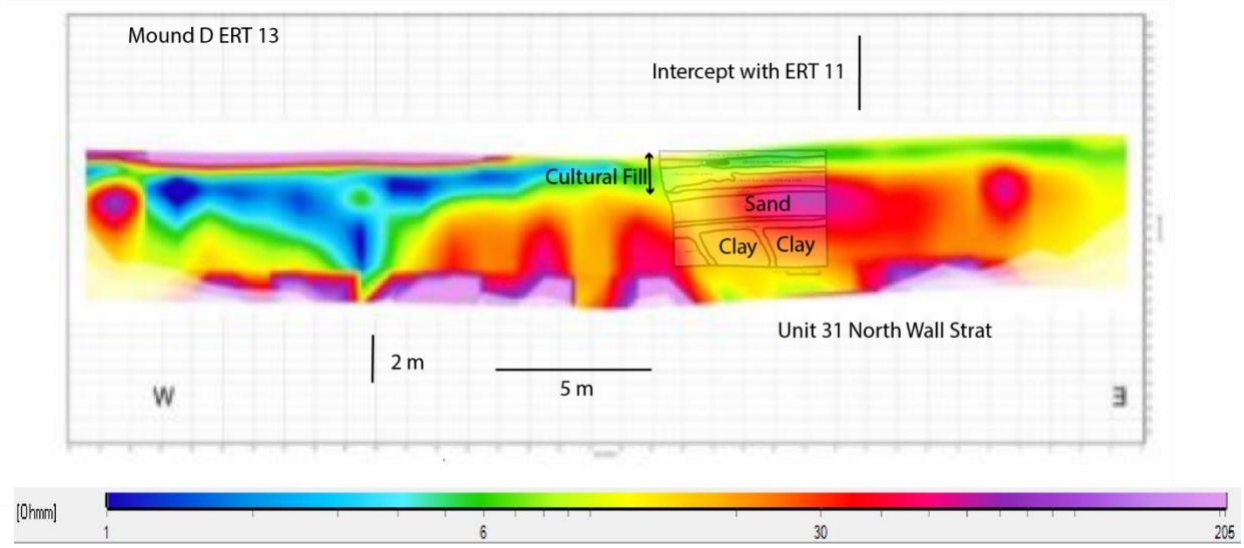

Figure 7. ERT Profile 13 and Mound D Stratigraphy: ERT Profile 13 was reflected to show the same orientation as the mound stratigraphy. The Mound D stratigraphy was overlaid onto the ERT data to show the correlation of the stratigraphic column with the layers seen in the ERT data.

Profile 16 shows Mound D from 80-110 H m, with the area of interest in relation to unit 31 being 82-94 m H. The bright purple on the surface is likely a signal caused by poor conduction between pins when running the survey. Approximately 1 m V into the mound is a lower resistivity layer, which may be the cultural and natural clay layers. Below the lower resistivity layer is a 2 m V high resistivity layer, which could be the aeolian sand layer.

The remaining two ERT profiles, 11 and 12, cannot be used to form a relationship between the ERT data and excavation pit stratigraphy. On profile 11, the pit area of the profile was too close to the edge of the survey. Since ERT data are collected in a trapezoid, there was not enough resolution on the end of profile 11 to highlight the different sediment layers of Mound D (figure 8). Profile 11 was able to detect two walls, which appear on the data set at identical spots of lower resistivity. These two green spots may be adobe walls. Since profile 12 was not corrected for topography, the stratigraphic layers in Mound D cannot be determined. Applying elevation changes to the ERT data will change how the resistivity values look in the subsurface.

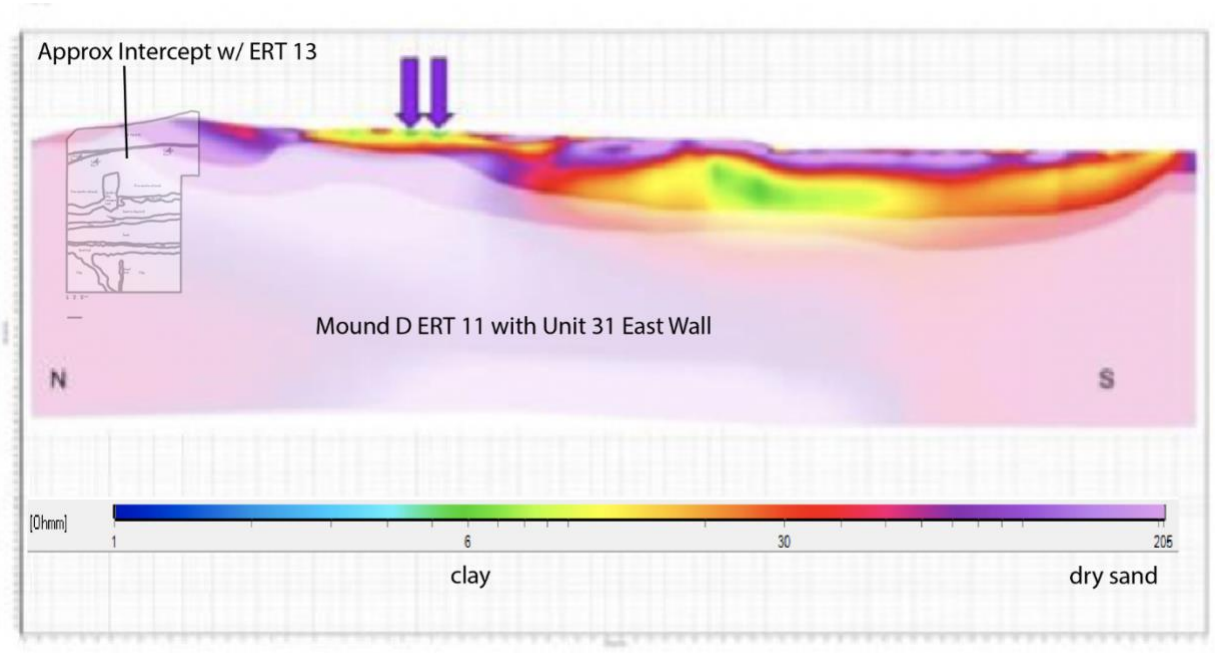

Figure 8. ERT Profile 11 and Mound D Stratigraphy: Unit 32 East Wall is overlaid onto ERT profile 11. The unit 31 excavation falls outside the trapezoid of data collection on ERT profile 11.

Mound B: Mound-Within-Mound

At Mound B, the abrupt shift in resistivity signal may indicate a change in composition of mound building material. Orange pins were plotted on the ERT profiles in Google Earth that correlate to the location of the orange arrows on the ERT data profiles

(figure 6). The orange pins were then connected to create a boundary of the mound-within-mound structure. Figure 9 shows the boundary between the mounds as the red profile connecting the orange pins. The younger mound is to the west of the profile and the older core mound is on the east side of the profile. Distinct changes in composition and the similar resistivity patterns displayed in profiles 17 and 20 present the strongest evidence for the burial of an older mound. The two orange arrows, indicating two locations where the mound composition changes, suggest the older core portion of the mound lies between the two orange arrows, from 24-43 m H, on profile 19.

The adobe wall was observed in the field as the mound was eroding away and revealing the adobe bricks which have a lower resistivity signal than the surrounding mound material. Profiles 17 and 20 reveal the lower resistivity readings of the adobe wall and are marked by the purple arrows (figure 6A and 6B respectively). The resistivity signature of the adobe wall in profile 17 appears to have a similar structure to the resistivity signal of the older core mound in profile 20. An interpretation of these data could be that the older portion of the mound consisted of more permanent structures, like adobe walls, compared to the newer portion of the mound. In the younger mound, the red and purple resistivity signal is more homogenous, possibly suggesting less structure. The new, younger mound may be made of a more sand rich material, which would explain the higher resistivity values, and was built up around the old mound in order to create a base foundation for the new, taller mound. The change in resistivity could be caused by either a change in building material or a different mound construction technique.

Irrigation of the farm fields surrounding Mound B is responsible for the small areas of higher resistivity along the edges of the mounds. These are the signals marked by

the blue arrows on profiles 17, 18, and 19 (figure 6 A, C, and D). The yellow arrow on profile 19 (figure 6D) at 57 m H matches the location of a brick wall that runs through Mound B. This is most likely the cause of the lower resistivity signal seen in the subsurface at this location. From 8-13 m H, there is a blue signal indicating a material with lower resistivity on profile 19. The road that runs next to Mound B is made of sand and gravel, giving this section of ground before the mound a lower resistivity value.

One possible reason for the lower resistivity difference between the mounds seen on profile 18 is due to increased anthropogenic disturbance. Profile 18 was run right over the road, so that area of the mound had been continually flattened, and had material removed from the mound to maintain the road. It is possible that the variation in resistivity in profile 18 is caused by anthropogenic alterations to the mound and is not an indication of the mound with mound structure. Profile 19 also runs over the highly disturbed northern portion of the mound, possibly explaining the weak resistivity changes observed. The anthropogenic changes to the mound make it challenging to determine the structure of the mound from 50-70 m H on profile 19. Another issue with the data is that the resistivity change observed at 24 m H does not match the mound boundary location indicated by profile 20. There is also an issue with the topography of profile 19. The lower resistivity area indicating the road around the mound should be at a lower elevation than the mound, but Figure 6D shows the road signal having the same elevation as the mound. The error occurred either in data collection or when the topography data were applied during post-processing.

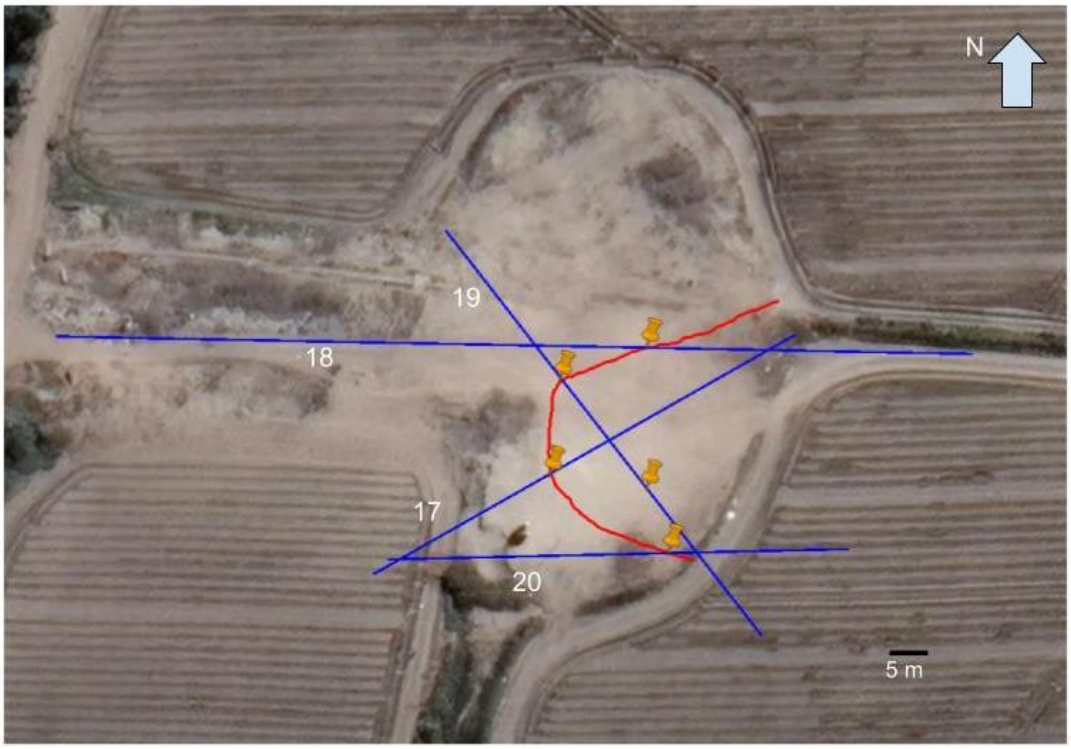

Figure 9. Map of Mound-Within-Mound Boundary on Mound B: The orange pins indicate places where the mound divide was seen in the ERT data. The red profile is the proposed old and new mound boundary location.

CONCLUSION

The earth resistivity tomography data collected in the ten survey profiles offered new insight into the subsurface structures on Mounds B and D at the Pozuelo site. Correlating the ERT data collected over Mound D to the stratigraphy observed in unit 31 proved to be challenging. Due to the resolution of the ERT profiles and the inability to use two of the profiles run over Mound D, a correlation with the unit 31 stratigraphy was made only using ERT profile 13. Certain sections of the ERT data on profiles 13 and 16 appear to have a similar resistivity pattern to how the inferred resistivity of the stratigraphic layers in Mound D should appear. However, the depths of the layers were not consistent. Future research at the Pozuelo site should rerun the survey profiles over Mound D with a shallower depth of penetration and longer profiles to create a high resolution profile of the Mound D subsurface. Continued research should relate the layers identified in the reprocessed profiles to the original data profiles, and then use the topography data collected to try and determine regional continuity in the subsurface.

A proposed mound-within-mound boundary was established using the four ERT profiles run over Mound B. The survey profiles displayed varying levels of resistivity change that allowed for the boundary between the old core mound and the new mound to be drawn. A limitation of this research was the anthropogenic damage done to Mound B through agriculture. The agriculture in the area disrupted the resistivity signals in certain portions of the ERT profiles. To confirm the location of the mound-within-mound boundary, future research should excavate pits on either side of the proposed divide. If distinctive pottery pointing to an earlier occupation is found in the older core portion of Mound B and a younger distinctive pottery is found in the new portion of the mound, this

would confirm the mound-within-mound hypothesis. Radiocarbon dates differing in age between the old and new mound would also serve to prove there is a buried older mound hidden in Mound B.

BIBLIOGRAPHY

Atwood, Roger. “Weaving For Their Ancestors.” *Archaeology*, Nov. 2020.

Burger, Henry Robert, et al. *Introduction to Applied Geophysics: Exploring the Shallow Subsurface*. W.W. Norton, 2006.

DeLeonardis, Lisa. “Early Paracas Cultural Contexts: New Evidence from Callango.” *Andean Past*, vol. 7. article 7. 2005.

Di Maio, Rosa, et al. “3D Reconstruction of Buried Structures from Magnetic, Electromagnetic and ERT Data: Example from the Archaeological Site of Phaistos (Crete, Greece): EM Prospecting at Phaistos.” *Archaeological Prospection*, vol. 23, no. 1, Jan. 2016, pp. 3–13. *DOI.org (Crossref)*, https://doi.org/10.1002/arp.1516.

Drahor, M.G., et al. “3D Resistivity Imaging from an Archaeological Site in South-Western Anatolia, Turkey: A Case Study.” *Near Surface Geophysics*, vol. 5, no. 3, June 2007, pp. 195–201. *DOI.org (Crossref)*, https://doi.org/10.3997/1873-0604.2006031.

Drahor, M. G., et al. “Magnetic and Electrical Resistivity Tomography Investigations in a Roman Legionary Camp Site (Legio IV Scythica) in Zeugma, Southeastern Anatolia, Turkey.” *Archaeological Prospection*, vol. 15, no. 3, July 2008, pp. 159–86. *DOI.org (Crossref)*, https://doi.org/10.1002/arp.332.

Kvamme, Kenneth L. “Integrating Multidimensional Geophysical Data.” *Archaeological Prospection*, vol. 13, no. 1, Jan. 2006, pp. 57–72. *DOI.org (Crossref)*, https://doi.org/10.1002/arp.268.

L. Nuzzo, et al. “Application of 3D Visualization Techniques in the Analysis of GPR Data for Archaeology.” *Annals of Geophysics*, vol. 45, no. 2, Dec. 2009. *DOI.org (Crossref)*, https://doi.org/10.4401/ag-3517.

Lascano, Eugenia, et al. “Geophysical Prospection at Floridablanca Archaeological Site, San Julian Bay, Argentina.” *Archaeological Prospection*, vol. 10, no. 3, July 2003, pp. 175–92. *DOI.org (Crossref)*, https://doi.org/10.1002/arp.213.

Linford, Neil. “The Application of Geophysical Methods to Archaeological Prospection.” *Reports on Progress in Physics*, vol. 69, no. 7, July 2006, pp. 2205–57. *DOI.org (Crossref)*, https://doi.org/10.1088/0034-4885/69/7/R04.

Osella, Ana, et al. “3D Electrical Imaging of an Archaeological Site Using Electrical and Electromagnetic Methods.” *GEOPHYSICS*, vol. 70, no. 4, July 2005, pp. G101–07. *DOI.org (Crossref)*, https://doi.org/10.1190/1.1993727.

Papadopoulos, Nikos G., et al. “Electrical Resistivity Tomography for the Modelling of Cultural Deposits and Geomophological Landscapes at Neolithic Sites: A Case Study from Southeastern Hungary: Electrical Resistivity Tomography in Palaeoenvironmental Modelling.” *Archaeological Prospection*, vol. 21, no. 3, July 2014, pp. 169–83. *DOI.org (Crossref)*, https://doi.org/10.1002/arp.1480.

Silverman, Helaine. “The Formative Period on the South Coast of Peru: A Critical Review.” *Journal of World Prehistory*, vol. 10, no. 2, 1996, pp. 95–146.

Strong, William D. “Paracas, Nazca, and Tiahunacoid Cultural Relationships in South Coastal Peru.” *Memoirs of the Society for American Archaeology*, no. 13, 1957, pp. 1–48.

Tantaleán, Henry, et al. “The Final Days of Paracas in Cerro Del Gentil, Chincha Valley, Peru.” *PLOS ONE*, edited by John P. Hart, vol. 11, no. 5, May 2016, p. e0153465. *DOI.org (Crossref)*, https://doi.org/10.1371/journal.pone.0153465.

---. “The Paracas Society of Prehispanic Peru.” *Oxford Research Encyclopedia of Latin American History*, by Henry Tantaleán, Oxford University Press, 2021. *DOI.org (Crossref)*, https://doi.org/10.1093/acrefore/9780199366439.013.981.

Viberg, Andreas, et al. “A Review of the Use of Geophysical Archaeological Prospection in Sweden.” *Archaeological Prospection*, vol. 18, no. 1, Jan. 2011, pp. 43–56. *DOI.org (Crossref)*, https://doi.org/10.1002/arp.401.

Young, Charles T., and David R. Droege. “Archaeological Applications of Resistivity and Magnetic Methods at Fort Wilkins State Park, Michigan.” *GEOPHYSICS*, vol. 51, no. 3, Mar. 1986, pp. 568–75. *DOI.org (Crossref)*, https://doi.org/10.1190/1.1442111.

Zheng, Wenfeng, et al. “Applications of Integrated Geophysical Method in Archaeological Surveys of the Ancient Shu Ruins.” *Journal of Archaeological Science*, vol. 40, no. 1, Jan. 2013, pp. 166–75. *DOI.org (Crossref)*, https://doi.org/10.1016/j.jas.2012.08.022.

APPENDIX: SUPPLEMENTAL DATA

Original ERT profile 13

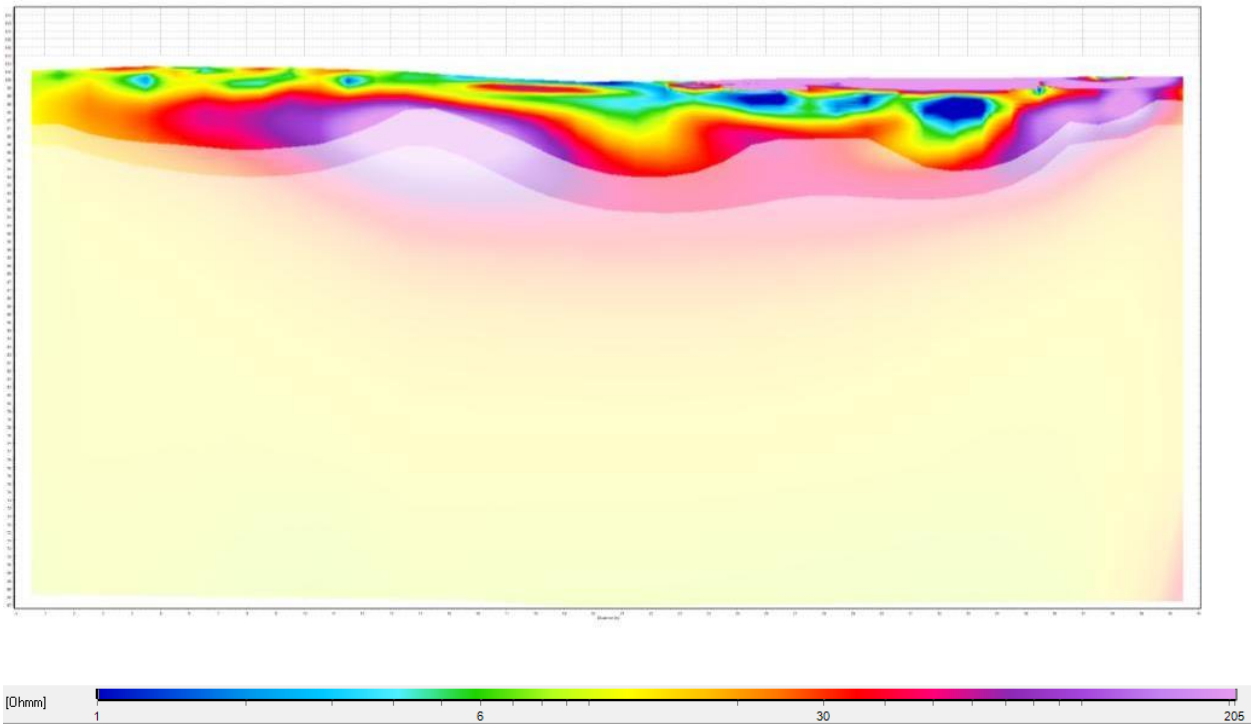

Original ERT profile 15

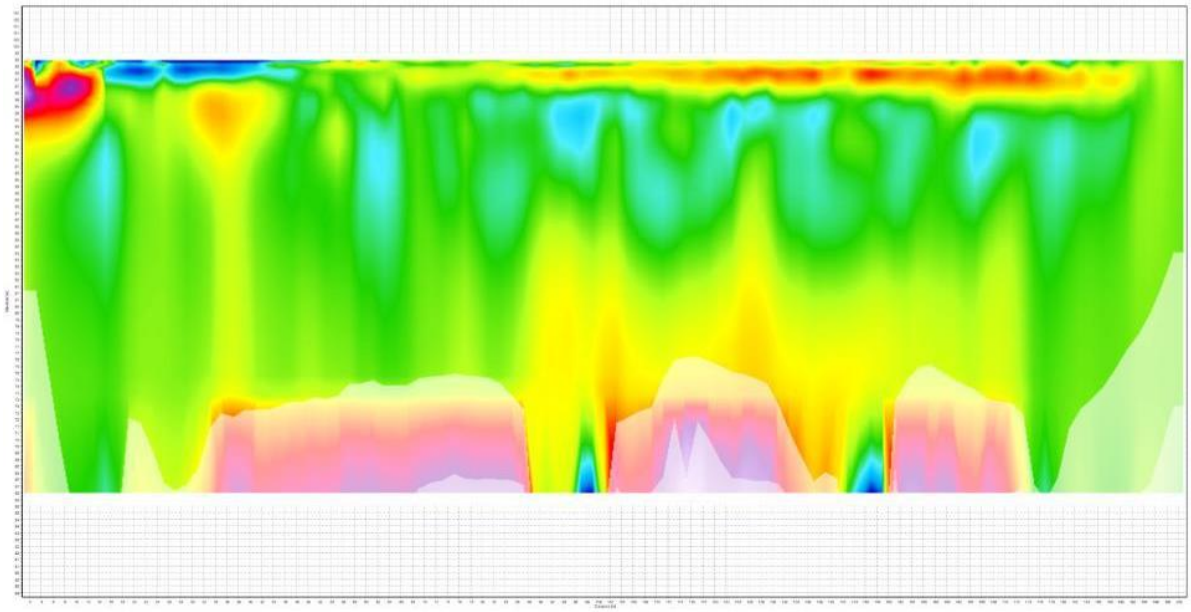

Reprocessed ERT profile 15

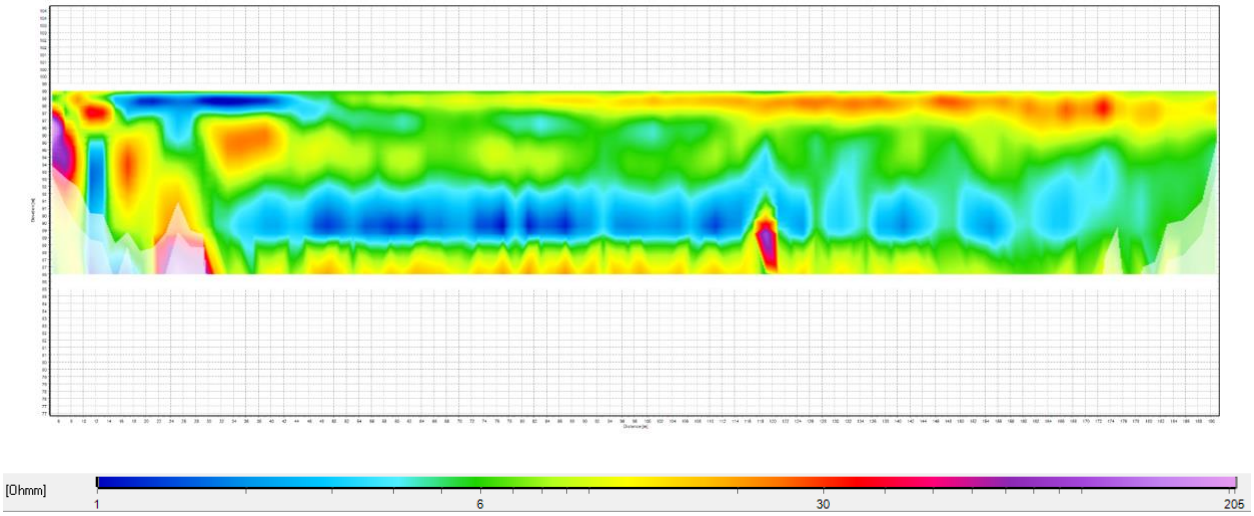

Original ERT profile 16

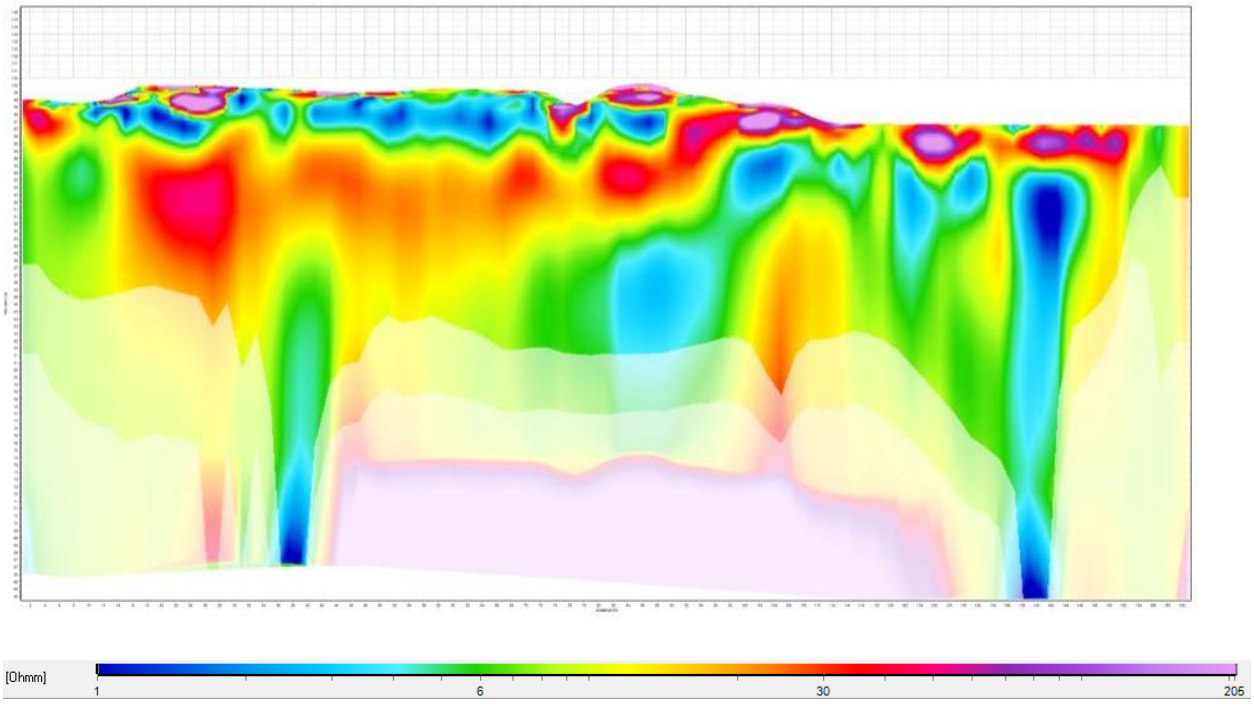

Original ERT profile 17

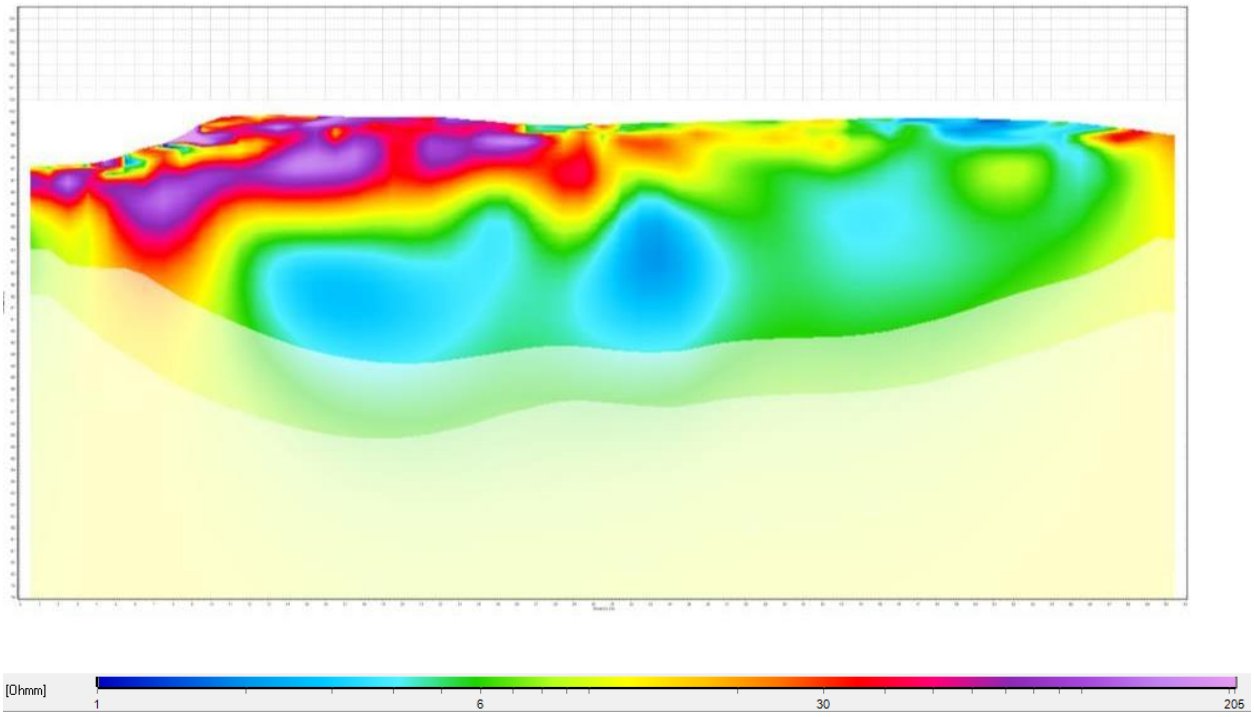

Original ERT profile 18

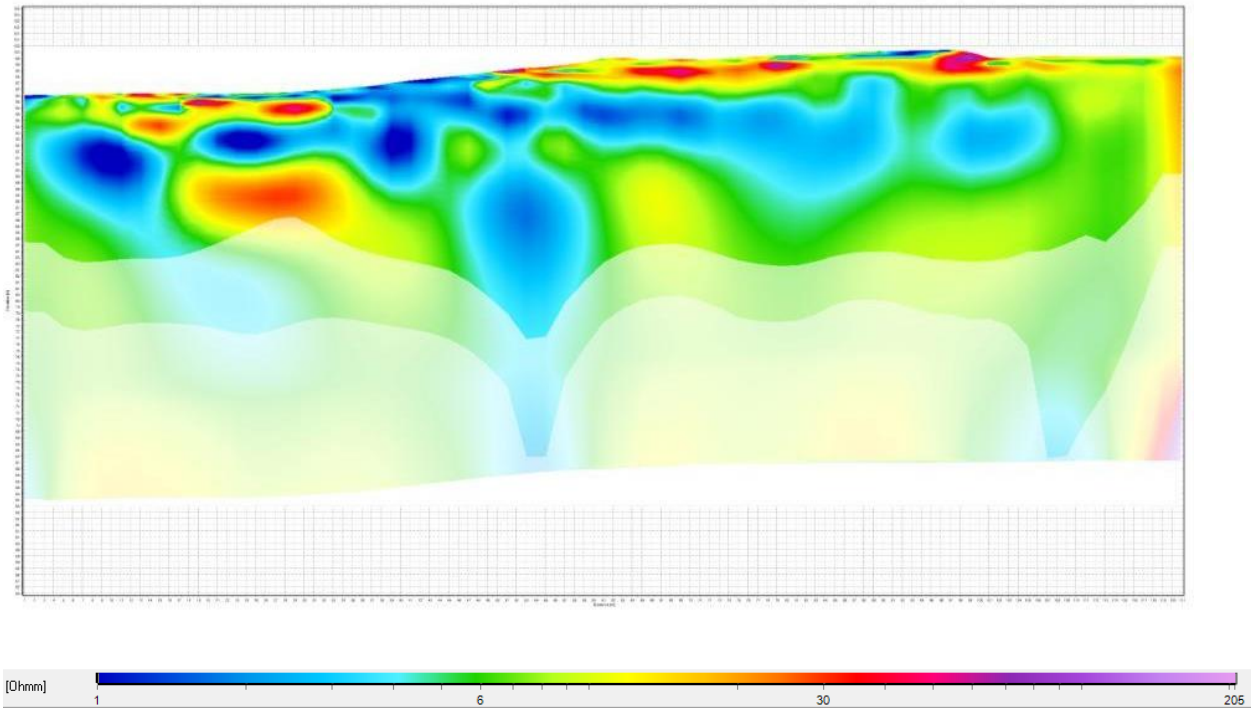

Original ERT profile 19

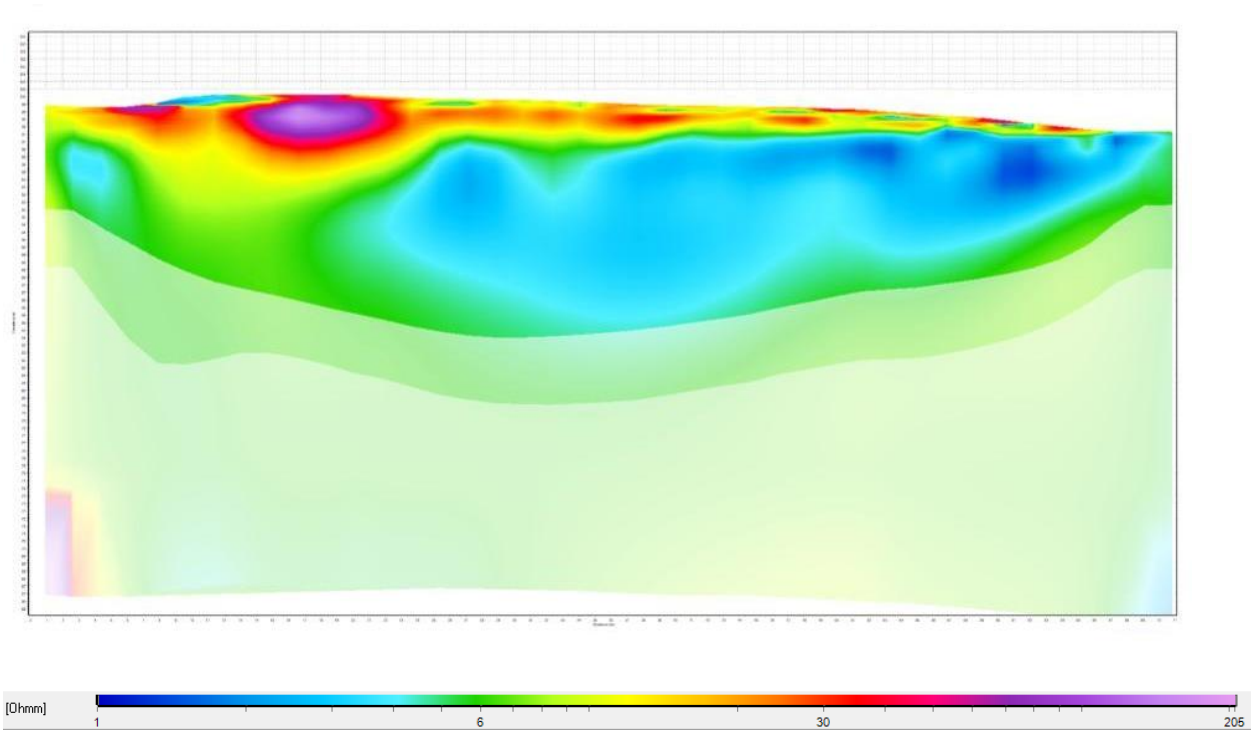

Original ERT profile 20

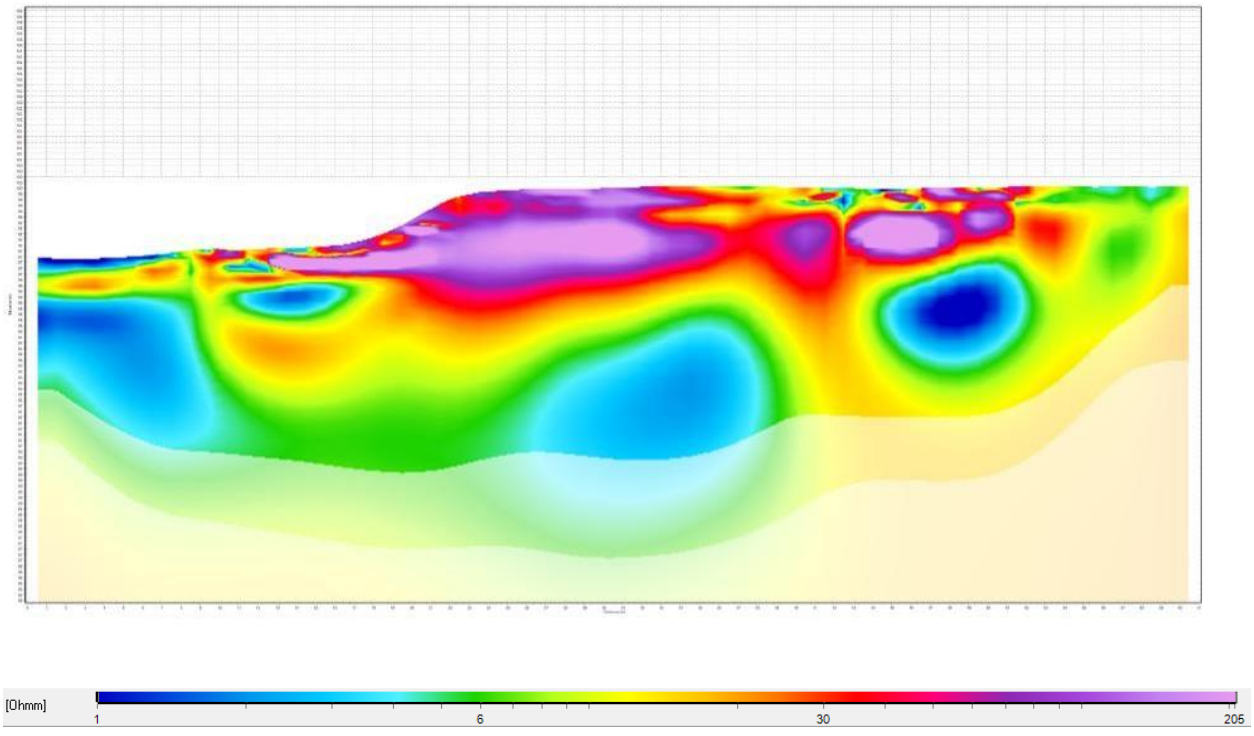

AUTHOR'S BIOGRAPHY

Caeli Connolly is an undergraduate at the University of Maine pursuing a Bachelor of Science degree in Earth and Climate Sciences with a concentration in Earth Science and a minor in Archaeology. She is also in the Honors College. Originally from Pennsylvania, Caeli came to UMaine to explore geoarchaeology. As an active member of the undergraduate geology club, Caeli served as the club secretary her junior year and the club president her senior year of college. Caeli has also served as a resident assistant for three years and has worked as a lifeguard for Campus Recreation for four years. She is a two year member of the Honor Society of Phi Kappa Phi.